JOURNAL OF CATALYSIS 36, 36–47 (1975)

Studies on Pore Structure of Adsorbents and Catalysts

III. Comparison of Pore Size Distributions Determined in Chrysotile and Zirconia Samples by Mercury Porosimetry and Nitrogen Capillary Condensation

L. A. DE WIT AND J. J. F. SCHOLTEN*

Department of Chemical Technology, Delft University of Technology, Julianalaan 136, Delft-2208, The Netherlands

Received May 6, 1974

Pore size distributions in iron oxide-chromium oxide, compressed Aerosil, zirconia powder, and loosely packed and compressed chrysotile have been determined by nitrogen capillary condensation (corrected Kelvin equation) and mercury penetration.

In all samples except zirconia, the pore-volume vs pore-radius distributions determined by mercury penetration showed no overlap with those found from nitrogen capillary condensation, mercury penetration yielding distributions located at a 30–40% lower level of the pore radii.

Following a discussion of the theoretical aspects and the experimental procedures and results, suggestions are advanced for explaining the discrepancies observed.

INTRODUCTION

Since the advent of automatic apparatus for determining pore size distributions from mercury penetration, the application of this method to the study of the pore structure of adsorbents and heterogeneous catalysts has increased sharply. A good description of the design of this equipment can be found in an article by Guyer, Böhlen, and Guyer (*1*). Now that mercury porosimeters are available that can be operated at pressures up to 3000 atm, it has become possible to determine distributions within a broad range of pore sizes, viz., between 7.5×10^5 Å (at 0.1 atm pressure) and 25 Å (at 3000 atm pressure).

Compared with methods such as nitrogen capillary condensation, mercury porosimetry offers several advantages, including high speed, large measuring range, and simple theoretical analysis of the results. On the other hand, the method is destructive, in the sense that in most cases only part of the mercury can be retracted from the pore system. Sometimes, however, the mercury can be removed by distillation.

Earlier investigators, including Ritter and Erich (*2*), Joyner, Barrett, and Skold (*3*), and Zwietering *et al.* (*4–6*), already wondered how far the experimental results agree with the information from nitrogen capillary condensation; in general a reasonable agreement is reported. This question has become of interest again for three reasons:

Whereas previously the range accessible to both methods reached from 75 to 500 Å, new developments in nitrogen capillary condensation (*7*) and mercury porosimetry (see above) have shifted the limits to 20 and 1000 Å, respectively.

Whereas in earlier comparative research nitrogen capillary condensation was described with the classical Kelvin equa-

* To whom all correspondence should be directed.

tion, the theoretical work by Broekhoff (7), together with our own experimental arguments (Part II of this series (25)) have disclosed that, especially in the range of pore sizes below 1000 Å, the discrepancy between the radii calculated with the classical Kelvin equation and the actual radii is rather large, i.e., 10–30%. This makes it necessary to reconsider the agreement reported earlier.

The question as to how far the two methods overlap calls for a more differentiated approach. In these considerations attention should be given to the size of the pore radius, the degree to which the pore model used in the analysis agrees with reality, and the amount of "interconnectivity" between the pores.

In this publication it will be demonstrated that the overlap of the pore distribution curves calculated from nitrogen capillary condensation and mercury penetration is not always as good as was supposed previously. Furthermore, it will be shown that the applicability of mercury porosimetry in the range of pore radii below 50 Å is open to doubt, but at the same time it raises interesting theoretical questions.

Theory

When mercury is forced into a porous solid (see Fig. 1), energy is expended in creating an intruding mercury surface. The interfacial free energy change dF_1 for an infinitesimal reversible increase of surface area under isothermal conditions is given by

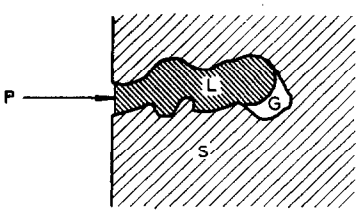

Fig. 1. Schematic representation of the intrusion of mercury into a porous solid. P is the intrusion pressure, L represents liquid mercury, G mercury vapor, and S the solid porous material.

$$dF_1 = \gamma_{L,S} \cdot dS_{L,S} + \gamma_{G,S} \cdot dS_{G,S} + \gamma_{L,G} \cdot dS_{L,G}, \quad (1)$$

where $\gamma_{L,S}$ is the free surface energy per unit area of the mercury–solid interface, $S_{L,S}$ the surface area of solid in contact with mercury, $\gamma_{G,S}$ the free surface energy per unit area of the gas–solid interface, $S_{G,S}$ the surface area of the gas–solid interface, $\gamma_{L,G}$ the free surface energy per unit area of the mercury in contact with the mercury vapor, and $S_{L,G}$ the surface area of mercury in contact with its vapor.

The energy dF_2 needed to force an infinitesimal volume dV of mercury into the porous solid in the case of reversible isothermal penetration is given by

$$dF_2 = P \cdot dV, \quad (2)$$

where P is the pressure at which the intrusion occurs.

Neglecting the very small amount of free energy spent in compensating for the production of heat during the intrusion of mercury (the heat of compression of mercury, and the friction heat at the mercury–solid interface), we have

$$dF_1 = dF_2, \quad (3)$$

or

$$P \cdot dV = \gamma_{L,S} \cdot dS_{L,S} + \gamma_{G,S} \cdot dS_{G,S} + \gamma_{L,G} \cdot dS_{L,G}. \quad (4)$$

During intrusion, the change in $S_{L,S}$ and $S_{G,S}$ is much greater than the change in $S_{L,G}$ corresponding to the change of the surface area of the mercury menisci; therefore, the last term in Eq. (4) may be neglected. Further, the Young–Laplace–Dupré law (7) states that

$$\gamma_{L,S} - \gamma_{G,S} = -\gamma_{L,G} \cos\theta, \quad (5)$$

where θ is the contact angle between the solid and the mercury. Since $dS_{L,S} = -dS_{G,S}$, combining Eqs. (4) and (5) gives

$$P \cdot dV = -dS_{L,S} \cdot \gamma_{L,G} \cdot \cos\theta. \quad (6)$$

For pores of circular cross-section and radius r, which are open at both ends or closed at one end

$$dV/dS_{L,S} = r/2. \quad (7)$$

Upon substitution of Eq. (7), Eq. (6) changes into

$$P = (-2\gamma_{L,G} \cdot \cos\theta)/r. \qquad (8)$$

This is the well-known Washburn relation, which was used for the first time by Ritter and Drake (*8*) for describing mercury penetration into porous substances and catalysts.

Applied to a pore system resembling a collection of tubular pores with circular constraints, or a collection of pores of ink-bottle shape, mercury penetration is governed by Eq. (8), and yields the distribution of the radii of the constraints, though the penetrated volumes are related to the volume of the pores or ink-bottles. Equation (8) is quite generally applied in the analysis of mercury penetration data, notwithstanding that the model of cylindrical pores is often very unrealistic.

For slit-shaped pores, or porous substances with microfissures giving access to cavities, $dV/dS_{L,S} = d/2$, where d is the width of the slit or the fissure. In such cases, Eq. (6) transforms into

$$P = (-2\gamma_{L,G} \cdot \cos\theta)/d. \qquad (9)$$

Compression of powders often results in pore systems resembling a more or less dense packing of nearly spherical particles. Penetration and retraction of mercury into and from such packings was studied by Kruyer (*9*), Frevel and Kressley (*10*), and Mayer and Stowe (*11, 12*).

The work of Mayer and Stowe is straightforward and directly applicable. These investigators define the pressure required for initial penetration (the "breakthrough pressure") in terms of the porosity ϵ of the spherical model and the contact angle θ of the mercury, and present calculated data relating to the ϵ-range from 25 to 50%, and to contact angles from 90° to 180° (see Table II in Mayer and Stowe's paper, Ref. *11*). The breakthrough pressure P of mercury in the access openings in a collection of nonporous uniform solid spheres is given by

$$P = \gamma_{L,G}(L'/A) \cdot 1/r_s, \qquad (10)$$

where r_s is the radius of the spheres. Mayer and Stowe calculated the function L'/A for all packings of spheres varying between the two extremes of three-dimensional close packing and three-dimensional cubic packing (see Tables II and III in their paper, Ref. *11*). From the measured breakthrough pressure P and the porosity ϵ, which may be determined, for instance, from the total amount of mercury intruded into the packing, r_s, the radius of the spheres, can be calculated. Otherwise, with P and r_s being known, the porosity can be found.

Kruyer (*9*) calculated the pressure–volume relationship for the early stage of *mercury retraction* from assemblies of uniform spheres, varying in packing-density from the closest-packed structure to primitive cubic packing: his results are in good agreement with those of Mayer and Stowe (*12*). If, after complete filling of the cavities with mercury, the pressure is decreased, the isolated mercury surfaces in the toroidal voids in the packing will ultimately interfere, and at that moment, according to Kruyer, the retreating mercury will set free the whole pore-space. This critical retraction pressure can be calculated from Table 2 in Kruyer's publication for various types of packing.

Little experimental information is available in the literature about the mercury retraction branch. Sometimes equilibration during retraction takes a very long time (even days or weeks), and in most cases a large portion of the mercury is not retracted at all (*11*). From a thermodynamic point of view, however, the retraction should continue as long as the penetrated mercury is in contact with the mercury outside the porous substance. For the most part, a portion of the mercury stays behind owing to rupturing of the mercury filaments in that part of the pore system where the constraints are narrowest, a phenomenon similar to that observed on cooling the mercury in the bulb of clinical thermometers.

Quantitative evaluation of Eqs. (8–10) calls for an exact knowledge of the surface tension of mercury, and of the contact angles between mercury and other materials. According to Young (*14*) the surface

TABLE 1
CONTACT ANGLES OF MERCURY ON SEVERAL SOLID SURFACES AT ROOM TEMPERATURE (EXCEPT WHEN OTHERWISE STATED)

Solid surface	Method of determination	Contact angle	Reference
Glass	Height-of-sessile-drop method	140°	(*14*)
Glass	Height-of-sessile-drop method	135°	(*18*)
Glass	Advancing and receding contact angles (both on tilted solid surface, at 18°C)	136.5°–141° 127°–126.5°	(*19*) (*19*)
Glass	Capillary depression	140°	(*20*)
Glass	Height-of-sessile-drop method	139°	(*21*)
Steatite	?	144.5°	(*17*)
Calcite	?	145.5°	(*17*)
Pyrite	?	145.7°	(*17*)
Parrafin wax	Advancing and receding contact angles (both on tilted solid surface)	137°–149° 134°–149°	(*17*) (*17*)
Cetyl alcohol	Advancing and receding contact angles, at 18°C	153°	(*21*)
Coconut charcoal	Capillary depression	180°	(*20*)
"Polymer spheres"	Breakthrough pressure	123°	(*10*)
Coal leaflets	Height-of-sessile-drop method	142°	(*21*)
Silicates (mica)	?	126°	(*22*)

tension is 485 ± 5 erg/cm² at 20°C. This is in good accordance with a recent observation by Roberts (*15*) who found 487 erg/cm² at 20°C for very pure mercury. The temperature coefficient of the surface tension of mercury ($d\gamma/dT$) is 0.21 erg/cm² deg, according to the same author.

Contact angles between mercury and various solid surfaces can be found in (*16*), and in Gmelin's "Handbuch der Anorganische Chemie" (*17*). Some values are listed in Table 1; it is seen here that $\theta = 140°$, the value used by most investigators, is a good mean, but also that large deviations may occur. If it is assumed that the angle of contact is 140° and the surface tension 480 erg/cm², Eq. (8) transforms to

$$r = 75{,}000/P, \qquad (11)$$

with r being expressed in Å and P in kg/cm². Equation (11) is quite generally used in mercury porosimetry, and also in this study.

Internal surface areas of porous solids can, according to Rootare (*23*), be calculated from mercury penetration, independently of the BET method. From Eq. (6) it follows that

$$S_{L,S} = -1/\gamma \cdot \cos\theta \cdot \int_0^{P_{max}} P \cdot dV, \qquad (12)$$

which, with $\gamma = 480$ dyne/cm and $\theta = 140°$, rearranges into

$$S_{L,S} = 0.267 \int_0^{P_{max}} P \cdot dV \quad (m^2/g), \qquad (13)$$

where P is in kg/cm², and dV in cm³/g. In this way the total surface area of the mercury-covered part of the solid is found. According to Rootare, and also according to the foregoing theory, the method leads to erroneous results when applied to strongly constrained pore systems.

In using Eq. (12) to calculate surface areas, the condition of reversible pore filling, assumed in its derivation, should be borne in mind, especially if the mercury penetration/retraction cycle shows hysteresis, which would be clear evidence for irreversibility.

EXPERIMENTAL

The experiments were carried out with a mercury porosimeter (trade mark Micromeritics Inst. Co., type 905-1), operating in the pressure range 0–3500 atm. Mercury was purified by single distillation.

Mercury penetration in a chrysotile sample was duplicated by means of a Carlo Erba type 70 H porosimeter, operating in the range 1–2000 atm. In this measurement the mercury was highly purified by dropping it through a glass column filled with 3 *N* nitric acid, followed by washing with distilled water and sulfur-free benzene, and drying; finally the mercury was distilled three times in an all-Pyrex apparatus.

The results obtained with the two types of porosimeters and the two grades of mercury agreed extremely closely, showing that the purity of the mercury used throughout this work was quite adequate for our purpose. All measurements were corrected for mercury compressibility (*16*).

Chrysotile, $Mg_3(OH)_4 \cdot Si_2O_5$, the properties and pore size distribution of which are described in Parts I and II (*24*, *25*), was divided into two portions. The first, sample B 1, was a loosely packed powder, whereas sample B 2 consisted of granules, strongly compressed at a pressure of 3500 kg/cm^2.

The zirconia sample, ZrO_2, obtained from Rijnten (*26*), was prepared by precipitation of $Zr(OH)_4$ from a solution of $ZrCl_4$, filtration, washing, drying at 120°C, and calcination at 450°C. The BET surface area was 64 m^2/g.

Using a Philips 300 M apparatus, we took an electron micrograph of the same zirconia sample, embedded in methyl methacrylate and sectioned into coupes of less than 500 Å thickness. The microscope was calibrated by means of a Rowland grid of 2160 lines/mm.

Results

(*a*) *Iron Oxide–Chromium Oxide Catalyst*

First of all we reanalyzed a comparative study by Zwietering *et al.* on nitrogen capillary condensation and mercury penetration in an Fe_3O_4–Cr_2O_3 sample (*4*, *5*). These workers prepared the catalyst by coprecipitation of the mixed oxides from a $Fe(NO_3)_3$–$Cr(NO_3)_3$ solution with Na_2CO_3. The precipitate was washed and dried at 110°C, and pressed to pellets of 3 × 3 mm. Reduction was performed in a mixture of 1 CO/5 H_2O at 350°C during 4 hr.

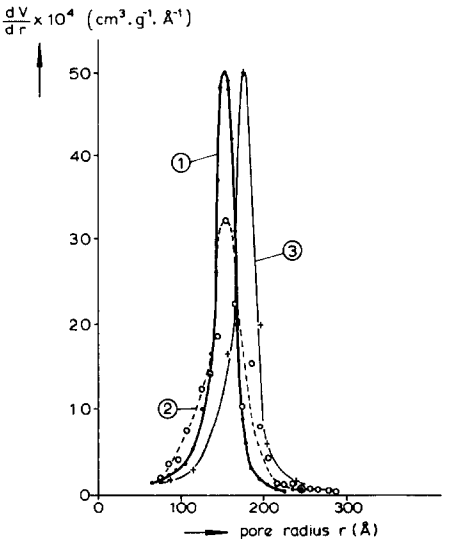

FIG. 2. Pore-size distribution in a Fe_3O_4–Cr_2O_3 catalyst. The derivative of the pore volume with respect to the pore radius is plotted as a function of the pore radius. Curve 1: found from nitrogen capillary condensation with the classical Kelvin equation. Curve 2: found from mercury penetration with the Washburn equation (γ = 480 dyne/cm, and θ = 140°). Curve 3: found from nitrogen capillary condensation, with the Kelvin equation corrected according to Broekhoff and de Boer.

The pore-size distribution curves, calculated on the assumption that the pores in the sample are circular in cross-section, and applying the classical Kelvin equation for nitrogen capillary condensation, and the Washburn relation (Eq. 11) for mercury penetration, are given in Fig. 2. The distributions obtained with the two methods show fair agreement (compare curves 1 and 2). We recalculated the nitrogen result by means of the Kelvin equation corrected according to Broekhoff (*7*); as is seen from Fig. 2 (compare curves 2 and 3) the agreement is then much worse. The top of the pore size distribution found from nitrogen capillary condensation lies at a 30% larger radius than the top of the distribution found from mercury penetration.

(*b*) *Compressed Aerosil Powder*

The second sample analyzed by Zwietering *et al.* (*5*) was prepared by compressing Aerosil powder (Degussa, Hanau, Germany) at a very high pressure. As re-

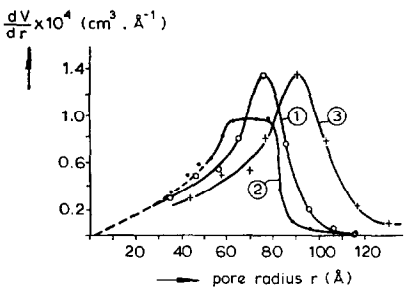

FIG. 3. Pore-size distribution in compressed Aerosil powder. Curve 1: found from nitrogen capillary condensation, with the classical Kelvin equation. Curve 2: found from mercury penetration with the Washburn equation (γ = 480 dyne/cm, and θ = 140°). Curve 3: found from nitrogen capillary condensation with the Kelvin equation corrected according to Broekhoff and de Boer.

vealed by electron microscopic investigation, the Aerosil consisted of nonporous, very smooth spherical particles of rather uniform size. The mean particle diameter is about 150 Å.

In Fig. 3 the pore size analysis as found from nitrogen desorption and from mercury penetration is plotted. In the calculation of curves 1–3 use is made of the circular cross section pore model, though we are sure that we are dealing here with a packing of nearly spherical particles. We see from the figure that application of the corrected Kelvin equation yields a distribution whose top lies 28% higher than the top in the mercury penetration distribution curve. This disagreement between the two methods is of the same order as found for the iron oxide–chromium oxide sample.

Since the packing consists of nearly spherical particles, Mayer and Stowe's relation (Eq. (10)) is applicable. From the texture data given by Zwietering *et al.* (*5*) the porosity of the pellets is found to be 51.8%, which points to a primitive cubic packing of spheres. From Table II in Mayer and Stowe's paper (*11*) it follows that the parameter L'/A in Eq. (10) is 3.80, assuming that the contact angle equals 140°. From the breakthrough branch of mercury starting at P = 938 kg/cm² and ending at 1500 kg/cm², minimum and maximum values of the sphere radii of 125 and 200 Å are found. The mean value (162 Å) corresponds with a particle diameter of 324 Å, which is about twice as high as the diameter observed in electron microscopy, viz. 150 Å. Hence, the choice of a more realistic pore model does not yield a better result.

(*c*) *Zirconia Powder*

Rijnten (*26*), in measuring the adsorption and desorption isotherms of his sample, found a typical A-type hysteresis loop, which, according to Broekhoff (*7*), should point to the presence of tubular pores of circular cross-section. However, our electron micrograph (Fig. 4) does not support this view: the preparation consists of a collection of very loosely packed interconnected crystallites, of rather uniform size and cubic to spherical shape. Rijnten measured a porosity of 51%. This value, which conforms to our EM observation, exceeds the theoretical figure for a primitive cubic packing of spheres (47.6%).

In Fig. 5 we have plotted the pore-size distribution calculated from the adsorption and desorption branches of the hysteresis loop of Rijnten's isotherm. Instead of the derivative of the cumulative pore volume with respect to the pore radius as a function of the pore radius (as presented in the other figures in this paper), we plotted the cumulative surface area as a function of the pore radius, assuming that the pores are circular, and applying the corrected Kelvin Eq. (7). It is seen that close agreement exists between the distributions found from the adsorption and desorption branches of the nitrogen isotherm.

Figure 6 represents the cumulative surface area as a function of the pore radius found by us from mercury penetration in the same sample. This curve agrees well with the results from the nitrogen method in Fig. 5.

We conclude that, notwithstanding the use of a wrong pore model in both methods (open circular pores), the agreement is very good in this case. This might be due to the fact that we are dealing here with a very loosely packed system in which the dimensions of the entrances of the cavities are practically equal to the dimensions of the cavities themselves.

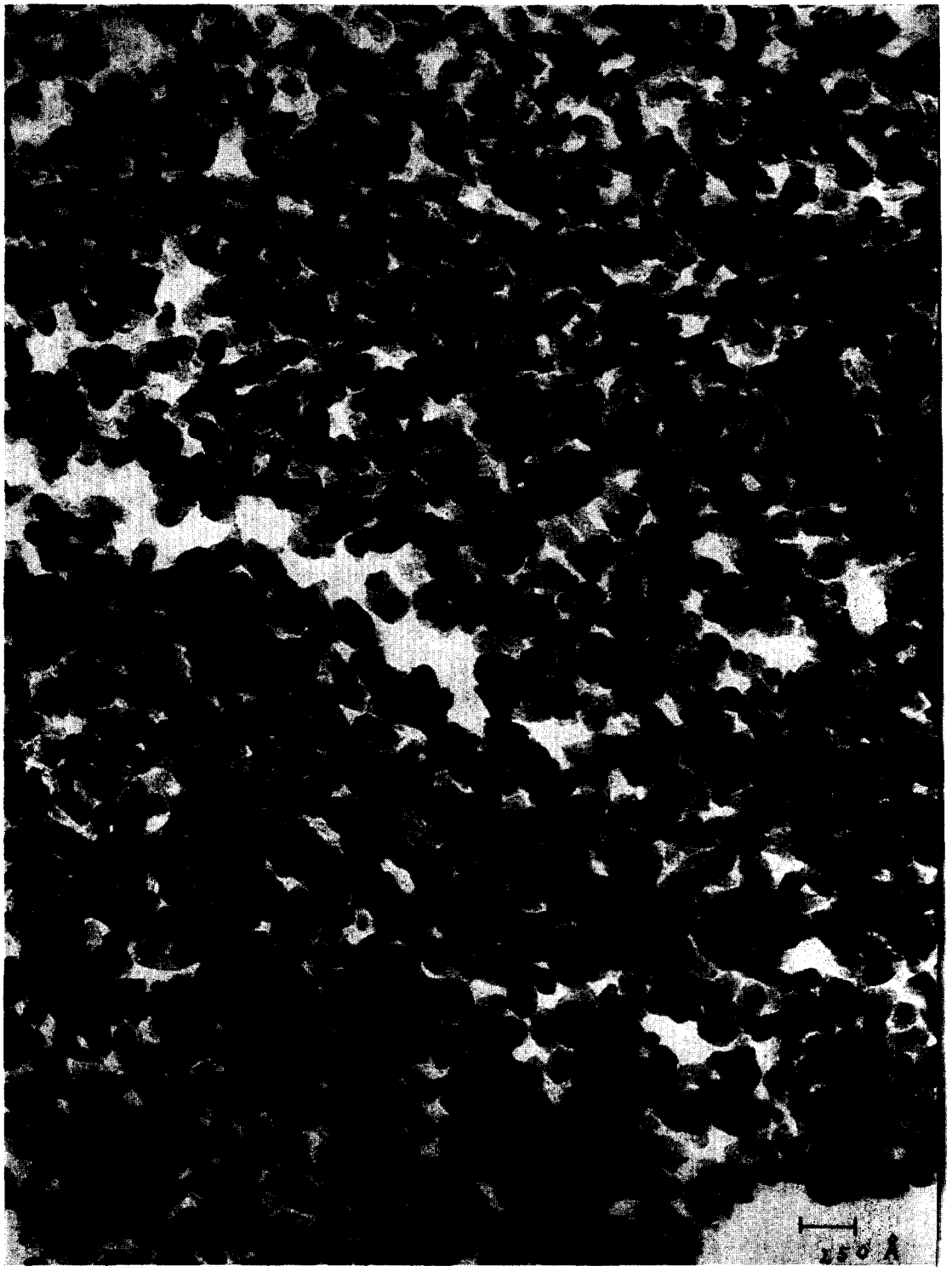

FIG. 4. Electron micrograph of zirconia powder, ZrO_2.

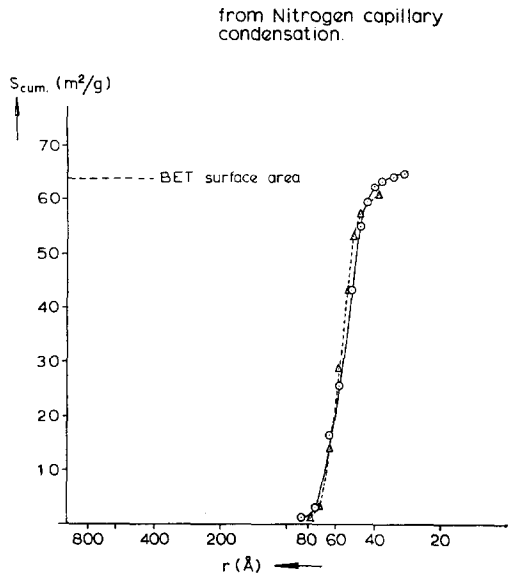

FIG. 5. The cumulative surface area of zirconia, as a function of the pore radius, calculated by applying the corrected Kelvin equation to the circular pore model. Open circles, starting from the desorption branch; open triangles, starting from the adsorption branch.

(*d*) *Chrysotile*

Figures 7 and 8 show the pore size distributions determined in chrysotile powder and compressed chrysotile powder by electron microscopy and nitrogen capillary condensation. These curves have been taken from the figures in Parts I and II (*24*, *25*), and are compared with those from mercury penetration plotted in the same figures.

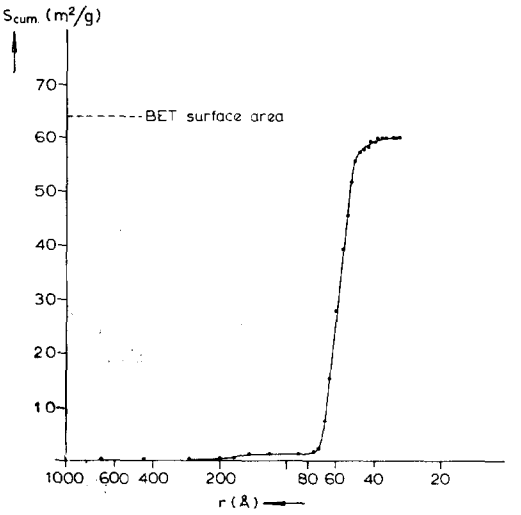

FIG. 6. Cumulative surface area of zirconia as a function of the pore radius, found from mercury porosimetry (circular pore model).

We shall first discuss the right-hand distribution peaks reflecting the distribution of cavities *in between* the hollow chrysotile needles. We see from Figs. 7 and 8 that the pore distributions calculated on the basis of the nitrogen and the mercury methods do not coincide, the mercury method giving 40% lower values for the peak radius of the distributions. Hence, just as found for iron oxide–chromium oxide and Aerosil, mercury porosimetry gives values for the radii which are much too low. It should be noted, however, that in both calculations the wrong pore model has been used, seeing that we are dealing with a packing of needles.

From Figs. 7 and 8 it can further be seen that the left-hand distribution peaks, corresponding to mercury penetration *into* the hollow chrysotile needles appear at radii one-third smaller than those found from EM and the nitrogen method. This is an unexpected feature since analysis of mercury penetration by means of the Washburn relation is fully justified now, for we are sure from EM observations (*24*) that we are dealing with perfectly cylindrical pores open at both ends. This point will be discussed in the next section.

Finally we remark that all pore size distributions found from nitrogen capillary condensation and discussed in this section, were calculated by means of the Barrett–Joyner–Halenda method (*27*); hence corrections are made for the thickness t of the adsorbed film.

DISCUSSION

In four out of five cases reported in this article where the pore size came in the range between 60 and 150 Å, the pore-size distribution calculated from mercury penetration does not coincide with the distribution found from nitrogen capillary condensation; in all these cases the radii determined by means of the mercury method are 30–40% too small. The pore

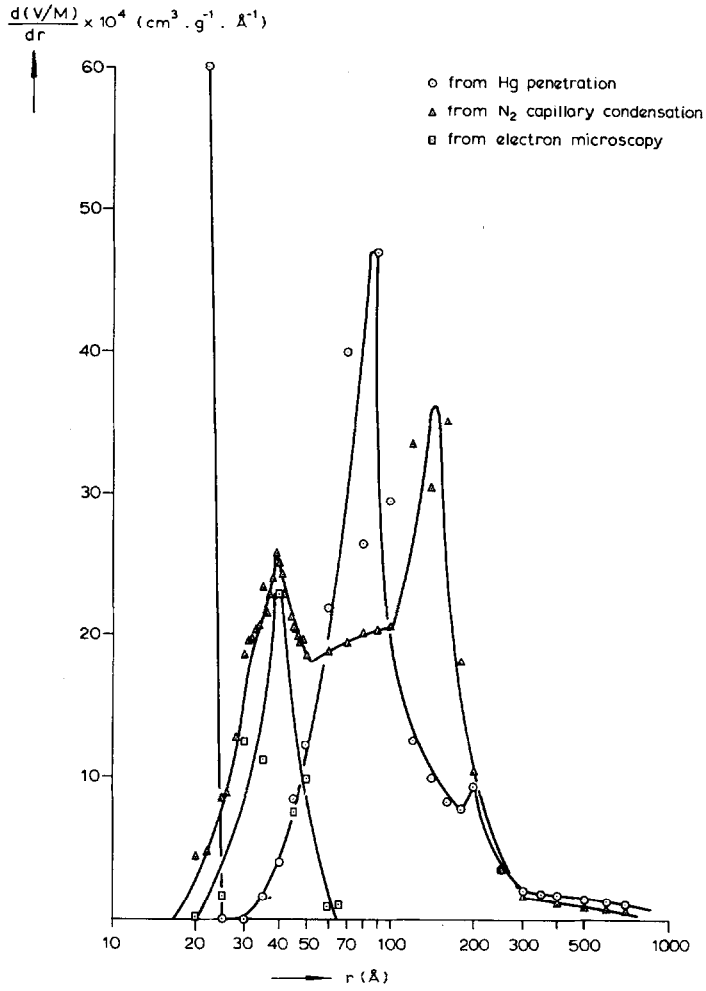

FIG. 7. Pore-size distribution in loosely packed chrysotile powder, sample B 1. The nitrogen isotherm was analyzed with the corrected Kelvin equation (desorption branch). The mercury penetration was analyzed with the Washburn relation. The derivative of the pore volume per unit mass towards the pore radius is shown as a function of the pore radius.

model used in the two analyses strongly deviated from reality, and this might be the cause of the discrepancies observed. However, in the case of compressed Aerosil, application of Mayer and Stowe's relation to a packing of spherical particles (which comes much closer to reality) still did not yield a better result.

The large discrepancy between the values from mercury penetration *into* the hollow chrysotile needles and the results of the other methods is not directly intelligible, seeing that we are dealing here with perfectly cylindrical pores. Moreover the result of the nitrogen method is in accordance with the EM observation (*25*), so that great certainty exists as to the real value of the radii. We will now examine what factors may be responsible for the nonvalidity of the Washburn relation in this case.

1. Contact Angle

From the Young–Laplace relation (5) we have (as $\gamma_{G,S}$ is very small)

$$-\cos\theta \simeq \frac{\gamma_{L,S}}{\gamma_{L,G}}. \qquad (14)$$

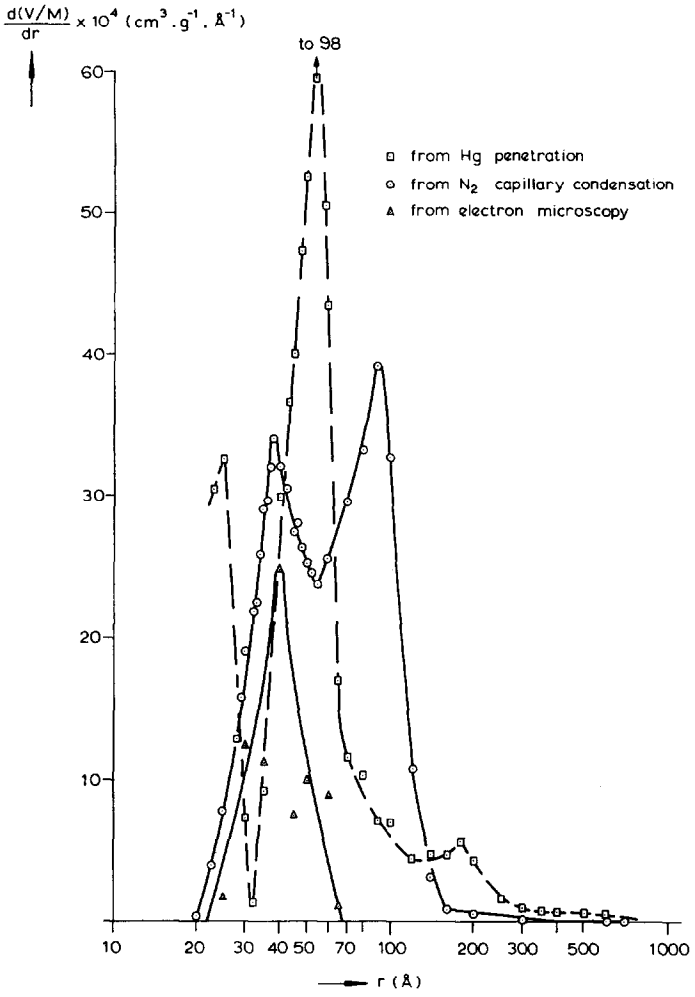

FIG. 8. Pore-size distribution in compressed granules of chrysotile, sample B 2. The analysis of the nitrogen isotherm (desorption branch) was made with the corrected Kelvin equation. The mercury penetration was analyzed with the Washburn relation. The derivative of the pore volume per unit mass with respect to the pore radius is shown as a function of the pore radius.

Hence, with $\theta = 180°$, $\gamma_{L,S} \simeq \gamma_{L,G}$, which would mean that the chrysotile wall has no influence on the mercury surface tension, or, expressed in another way, that the heat of adsorption of mercury is zero and chrysotile is totally unwetted by the mercury. Introduction of $\theta = 180°$ into the Washburn relation would bring our results into somewhat better, though not full, agreement with the EM and nitrogen results, but such a contact angle has never been found for mercury on silicates and hence must be regarded as very unlikely.

A contact angle of 126°, as experimentally established for mercury on silicates like mica (see Table 1), would be much more likely, although it must be pointed out that, owing to the strong concavity of the inner walls of the chrysotile needles (a radius of curvature of the order of 40 Å), the heat of adsorption of mercury will be greater than on a flat surface, with the consequence that the contact angle will be smaller still. Introduction of, for instance, $\theta = 120°$ into the Washburn equation shifts the top of the mercury distribution curves

in Figs. 7 and 8 to 16.3 Å and, hence, causes an even larger discrepancy between the mercury results and the EM and nitrogen figures.

2. Surface Tension γ

In our research the surface tension was taken to be 480 dynes/cm, a value which is quite generally accepted and applied in mercury porosimetry. However, its validity is limited to a flat mercury surface. Once the mercury has penetrated into the chrysotile needles, its surface becomes very strongly bent, the radius of curvature being of the order of 40 Å, and this strong bending will influence the value of γ.

The theory regarding the influence which the surface curvature has on surface tension is not very well developed. According to Gibbs (*28*) the theory loses its validity for radii with a curvature smaller than 100 Å. Since the surface tension is five to ten times that of the liquids considered in the Gibbs theory, one might expect that, applied to mercury, the thermodynamic approach will become invalid already at curvatures far in excess of 100 Å.

Benson and Shuttleworth (*29*) used elementary molecular arguments to show why the surface energy depends on the curvature, and made a rough estimate of this dependence; their treatment is appropriate to small nuclei for which the earlier treatments were not valid. They conclude that even for molecular clusters of thirteen molecules the surface energy will be less than 15% smaller than for a plane surface. However, their theory was set up for molecules showing van der Waals interaction only, and it is not at all sure that it is valid also for mercury clusters where strong chemical bonds exist between the atoms.

If the discrepancy in our measurements is due to the influence which curvature has on the surface tension, we have to conclude that for a convex mercury surface with a radius of curvature of 40 Å the surface tension is about 50% greater than for a flat surface. The discrepancy found between electron microscopic observation and the mercury intrusion analysis according to Mayer and Stowe in the case of Aerosil points to a surface tension for a concave mercury surface which is about 50% lower than for a flat surface.

Such adjustments of the surface tension would bring our results into good agreement with the EM and nitrogen results.

3. Start of Mercury Intrusion

The very first moment mercury penetrates into a circular tube of radius r, a hemispherical mercury meniscus is formed, the curvature of which is twice the curvature of the mercury in contact with the inner tube wall. Calculation of $dS_{L,G}/dV$ for the hemispherical mercury meniscus gives

$$\frac{dS_{L,G}}{dV} = \frac{P}{\gamma_{L,G}} = \frac{-2\cos\theta}{r}, \qquad (15)$$

which result is equivalent to the Washburn relation (*8*). It follows that formation of the meniscus proceeds at the same pressure as mercury intrusion itself and, hence, cannot be responsible for the higher intrusion pressure measured on the chrysotile needles.

4. Constraints and Blocking

Finally, the cause of the too high intrusion pressure might be sought in the presence of constraints, or in partial blocking of the pores in the needles. This, however, was not observed in the electron micrographs (see Fig. 1 in Ref. *24*).

In conclusion we may state that in practice we have to reckon with the possibility of relatively large discrepancies between the results from mercury penetration and nitrogen capillary condensation. Introduction of a more realistic pore model is necessary, but does not improve the agreement on dealing with very narrow capillaries. Looked at from the theoretical angle, it will be necessary to investigate in more detail how far the Washburn relation is applicable to narrow capillaries. One should bear in mind that in pores of, say, 40 Å radius no more than about 13 mercury atoms can be spread over the length of the radius, and this raises the question whether the thermodynamic theory and,

hence, the Washburn equation, are valid under these conditions (*28*).

In the experimental field more research will need to be done with respect to systems whose pore shape and pore dimensions are known from electron microscopy. We ourselves have planned to undertake further investigations on samples of *natural* chrysotile having a slightly larger mean inner pore radius than the synthetic material.

Acknowledgments

Thanks are due to Mr. A. M. Kiel who carried out the electron microscopic work, to Mr. J. Teunisse and Mr. N. van Westen for skilled experimental assistance, and to Mr. J. A. Konvalinka and Dr. J. C. Rasser for helpful discussions.

Stichting Scheikundig Onderzoek Nederland, a division of the Netherlands Organization for the Advancement of Pure Research (ZWO), supported this work.

References

1. Guyer, A., Böhlen, B., and Guyer, A., *Helv. Chim. Acta* **42**, 2103 (1959).

2. Ritter, H. L., and Erich, L. C., *Anal. Chem.* **20**, 665 (1948).

3. Joyner, L. C., Barrett, E. P., and Skold, R., *J. Amer. Chem. Soc.* **73**, 3155 (1951).

4. Zwietering, P., and Koks, H. L. T., *Nature (London)* **173**, 688 (1954).

5. Zwietering, P., van Montfoort, A., and Tebben, J. H., *in* "Tercera Reunión Internacional sobre Reactividad de los Sólidos," Section IV, pp. 123–137. Madrid, 1956.

6. Zwietering, P., *in* "The Structure and Properties of Porous Materials" (D. H. Everett, and F. S. Stone, Eds.), p. 287. Butterworth Scientific Publications, London, 1958.

7. Broekhoff, J. C. P., *in* "Physical and Chemical Aspects of Adsorbents and Catalysts" (B. C. Linsen, Ed.), Ch. I, pp. 1–59. Academic Press, London, 1970.

8. Ritter, H. L., and Drake, L. C., *Ind. Eng. Chem. Anal. Ed.* **17**, 787 (1945).

9. Kruyer, S., *Trans. Faraday Soc.* **54**, 1758 (1958).

10. Frevel, L. K., and Kressley, L. J., *Anal. Chem.* **35**, 1492 (1962).

11. Mayer, R. P., and Stowe, R. A., *J. Colloïd Sci.* **20**, 893 (1965).

12. Mayer, R. P., and Stowe, R. A., *J. Phys. Chem.* **70**, 3867 (1966).

13. Kamakin, N. M., *in* "Methoden der Strukturuntersuchung an Hochdispersen und porösen Stoffen," p. 73. Akademie-Verlag, Berlin, 1961.

14. Young, T. F., quoted by Adam, N. K., *in* "Physics and Chemistry of Surfaces," p. 185. Oxford University Press, London, 1944.

15. Roberts, N. K., *J. Chem. Soc.* 1907 (1964).

16. Scholten, J. J. F., *in* "Porous Carbon Solids" (R. L. Bond, Ed.), p. 225. Academic Press, London, 1967.

17. Gmelins Handbuch der Anorganische Chemie, Verlag Chemie, GMBH, Weinheim 1960. Edited by "der Deutsche Chemische Gesellschaft," Band No. 34, Teil A, p. 291, 1960.

18. Bate, T., *Phil. Mag.* **28**, 252 (1939).

19. Yarnold, G. D., *Proc. Phys. Soc.* **58**, 120 (1946).

20. Juhola, A. J., and Wiig, O., *J. Amer. Chem. Soc.* **71**, 2078 (1949).

21. Platschenov, T. C., Alexandrov, V. A., and Belozerkovski, G. M., *in* "Methoden der Strukturuntersuchung an Hochdispersen und porösen Stoffen," p. 88. Akademie-Verlag, Berlin, 1961.

22. Talmud, D. Z., *Z. Phys. Chem. Abt. A* **148**, 227 (1930).

23. Rootare, H. M., *J. Phys. Chem.* **71**, 2733 (1967).

24. Scholten, J. J. F., Beers, A. M., and Kiel, A. M., *J. Catal.* **36**, 23 (1974).

25. de Wit, L. A., and Scholten, J. J. F., *J. Catal.* **36**, 30 (1974).

26. Rijnten, H. Th., thesis Delft Technical University, Delft 1971, p. 38.

27. Barrett, E. P., Joyner, L. G., and Halenda, P. P., *J. Amer. Chem. Soc.* **73**, 373 (1951).

28. Gibbs, J. W., "Collected Works," Vol. I, p. 232. Longmans and Green, New York, 1928.

29. Benson, G. C., and Shuttleworth, R., *J. Chem. Phys.* **19**, 130 (1951).